Centrifugal Compressor in Aeroengine Application

R.S. Amano* and C. Xu†
University of Wisconsin-Milwaukee, Milwaukee, WI, 53201

This paper describes a new development of high efficiency and a large surge margin flow coefficient of 0.145 centrifugal compressor. A viscous turbomachinery optimal design method developed by the authors for axial flow machine was further extended and used in this centrifugal compressor design. The new compressor has three main parts: impeller, a low solidity diffuser and volute. The tip clearance is under a special consideration in this design to allow impeller insensitiveness to the clearance. A three-dimensional low solidity diffuser design method is proposed and applied to this design. This design demonstrated to be successful to extend the low solidarity diffusers to high-pressure ratio compressor. The design performance range showed the total to static efficiency of the compressor being about 85% and stability range over 35%. The experimental results showed that the test results are in good agreement with the design.

I. Introduction

A centrifugal compressor can be designed with much higher De Haller number than an axial compressor can achieve. Therefore, it is possible for a centrifugal compressor to have a much higher stage pressure ratio than axial ones. Centrifugal compressors have wide applications for a mass flow rate less than 10 kg/s [1, 5].

The low flow coefficient centrifugal compressors have wide applications in turbo shaft aircraft engines, petrochemical plants, and manufacturing. However, being in a low-power class, these compressors need to be inexpensive to manufacture and operate, requiring that the compressor having a simple design with less number of parts and a smaller relative tolerance. Moreover, the five-axial machine is now a common tool for impeller machining, but most other parts should be fabricated by using other type of machining to reduce the manufacturing costs.

Turbomachinery industries are interested in using optimization procedures that enable to enhance compressor efficiency and wide operating ranges. Turbomachine design normally starts with a meanline program at each individual operating point on a map, then throughflow calculation is performed, and finally, the impeller, diffuser and volute are designed. In this study, a recently developed turbomachinery viscous optimal method [6,7] especially for axial machines was further extended to a centrifugal compressor design. The main focus of this study lies in a development of a flow coefficient in the order of $\phi = 0.145$ compressor. The design requirements for this compressor development are that the compressor stage pressure ratio is 3.65 and a preferred flow rate is about 0.75 kg/s at the design condition with a total to static efficiency larger than 84% and the stability range SB≥30%. The compressor design employs a viscous process for achieving efficiency and stability targets. Good surge margins were achieved without use of a variable geometry for a steady-state operation. Special attention has been paid to a tip clearance during the impeller design. The compressor developed in this study consists of three major parts: an impeller, low solidity diffuser, and volute. In this study, particular attention was paid mainly on impeller and low solidity diffuser development.

II. Design Process

A centrifugal compressor stage consists of three main components: a rotating impeller, diffusers, and a volute as shown in Fig.2. The low flow coefficient impeller design is critical in terms of aerodynamic efficiency and operating range of the compressor stage.

A. Impeller Design

Impeller aerodynamics also impacts the performance of the diffuser and volute. It is very important to achieve an optimized configuration of the impeller. The traditional impeller design has been performed by using a one-dimensional analysis; then, the blade and endwall geometries were selected according to the standard criteria so that the new impeller has a scale of an exiting one. This design method could not provide the predication of the impeller flows in order to improve the design; therefore, the flow separation in the impeller is a necessary consequence of the stipulation of the impeller geometry in most cases.

---

* Professor, Department of Mechanical Engineering, P.O. Box 784, AIAA Associate Fellow.
† Associate, Department of Mechanical Engineering, P.O. Box 784.

In this study, one-dimensional studies were initially performed to do parameters studies. It was shown that the rotational speed at design condition of 65,000 rpm was necessary to achieve high compressor efficiency and to maintain overall diameter objectives. Due to the limitations of motor and structure, the design rotational speed was set to 59,000 rpm. The blade tip to hub ratio is about 0.34 and an inlet absolute tip Mach number is about 0.4, which results in the inlet relative tip Mach number, is about 0.9. The impeller was designed without splitter due to the size of the impeller and manufacturing restrictions. A high impeller backward exit angle was used in this design to improve the efficiency through the reduction of the impeller loading and to improve a surge margin by providing a steeper energy addition characteristic. The high impeller exit blade angles required a coordinated aeromechanical design effort.

The detailed flow structure and impeller performance were analyzed by using the Computational Fluid Dynamic (CFD) analysis to help a parametric study and an optimization. In order to perform the optimization, a number of geometrical parameters were identified. The design modifications were made by varying the values of such parameters. The final impeller was designed by using a fast three-dimensional viscous code [12].

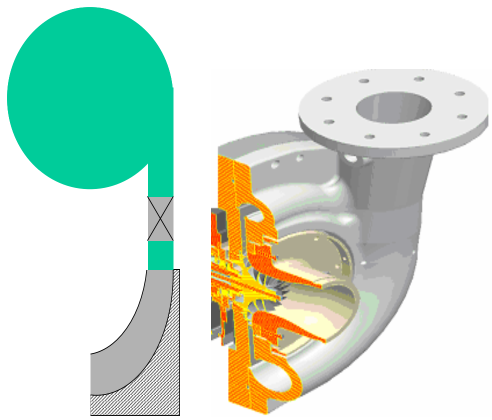

Figure 2. Cut away view

H-type of mesh [12,13], which is suitable for obtaining low-skewed grids around long and thin blades, was employed to compute the flow in a single blade passage. Grid sizes were chosen in order to accomplish a grid independent state to have enough accuracy and fast enough for design and optimization. After several preliminary studies it was shown that the computational grid size of 43×43×153 was grid-independent; and thus was used for all of the design simulations through this study. The typical meridional mesh is shown in Fig. 3.

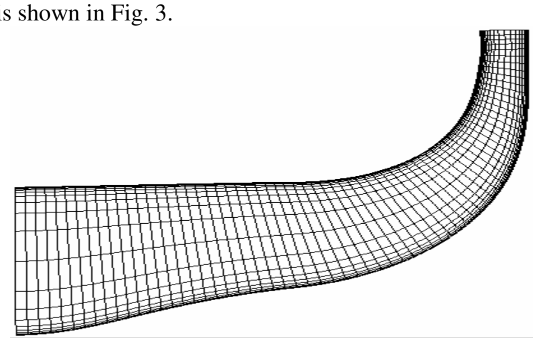

Figure 3. Mesh in meridional plane.
(Half of the mesh points are made visible)

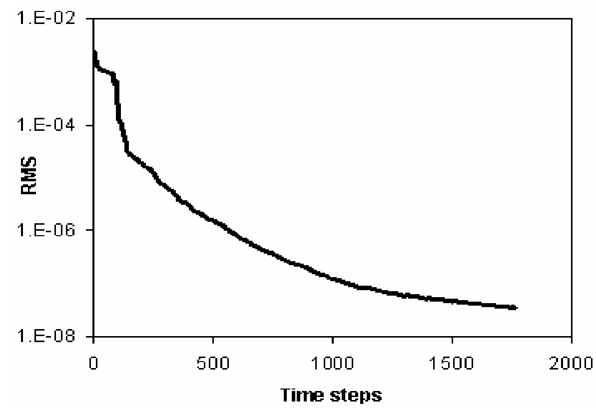

Figure 4. Convergence history.

The computation was carried out based on the single blade passage during the impeller design. After each calculation was done, a DOE Optimization study was performed [6, 7]. For every calculation, the convergence was set when the residual RMS level with at least a fifth order of magnitude reduction with respect to its initial value. The typical convergence history is shown in Fig. 4.

With several iterations of optimizations, the final impeller was designed. The meridional channel shape has characteristics at both inlet and exit with a straight channel and middle has relatively large curvature. The impeller hub and shroud relative-velocity distributions at design pressure ratio are shown in Fig. 5. The final blade has a backswept angle $\beta=56^o$. The final blade angle distributions at blade hub and shroud are shown in Fig. 6. The final blade angle was adjusted after the optimization study at design point. The impeller blade angle was set to about 3^o incidence at both tip and root sections in order to increase the choke margin. The blade angles at both shroud and hub combined with meridional channel shape provide the reasonable blade loading as shown in Fig. 6. The static pressure contour at mid meridional plane between two blades is shown in Fig. 7. The velocity vectors for the flow near the blade pressure-side and suction-side are shown in Figs. 8 and 9, where it is shown that the flows are well organized inside the impeller with only the small separation region appearing near the tip of the blade. Figure 10 shows the relative velocity vectors along the shroud surface near the impeller exit. It is depicted in this figure that a flow separation appears near the shroud tip region. Flow separations were induced by the large tip clearance (2% of the exit width) at the tip due to the blade-trailing wake and pressure gradient. Several efforts were made to eliminate flow separations. The variable tip clearance was used to reduce the separation. The reduction of the shroud loading and reduction of the blade trailing edge thickness showed the improvement of flows near the shroud tip ranges. However, the reduction of the shroud loading increased the hub loading which caused the flow separation at the hub. The reduction of the trailing edge thickness caused the mechanical stress and vibration frequency problems. Due to the limitation of the development time, current design was used as the final design. Variable clearance can reduce the affects of efficiency with the change in the axial tip clearance as shown in Fig. 10. As shown in Fig. 11, the low clearance sensitivity allows the impeller to operate up to 6% without dropping efficiency 3%. The variable tip clearance allows the impeller manufacturing having a relatively large tolerance and also renders impeller operational work in an extremely severe condition such as a fast rapid acceleration like turbocharger and a helicopter engine. The absolute flow angle contours at the rotor exit are shown in Fig. 12. As seen in this figure, only the flow region close to the tip entails a high flow angle. This is because the meridional velocity is very low in this region.

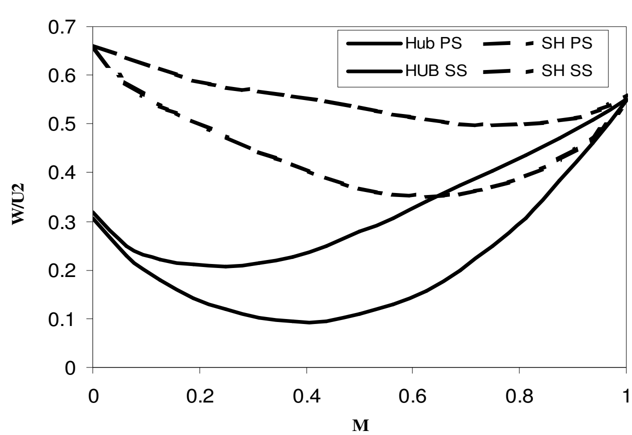

Figure 5. Blade surface velocity distributions.

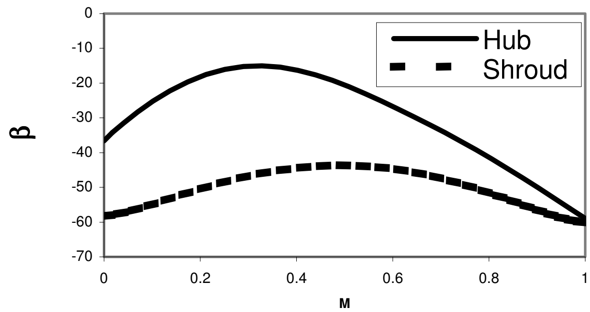

Figure 6. Blade angle distribution.

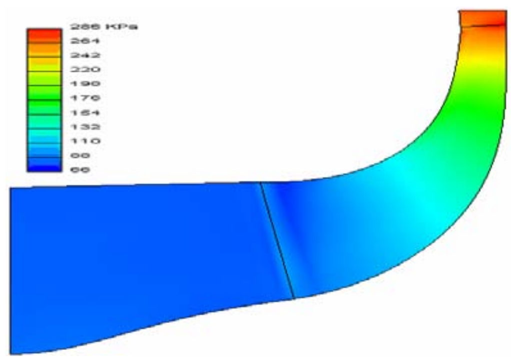

Figure 7. Static pressure distributions at mid-plane between two blades.

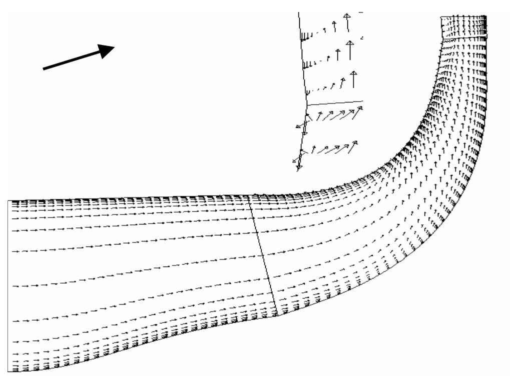

Figure 8. Velocity vectors near pressure surface.

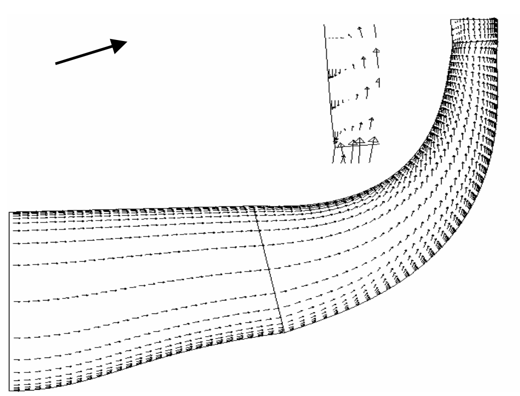

Figure 9. Velocity vectors near suction surface.

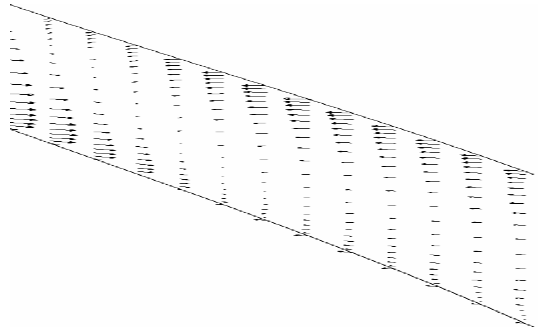

Figure 10. Relative velocity vectors near shroud surface.

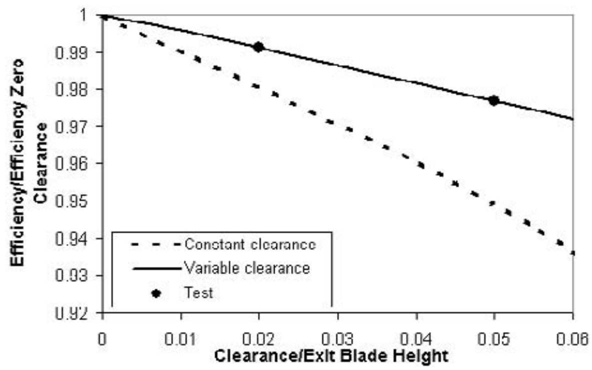

Figure 11. Tip clearance sensitivity.

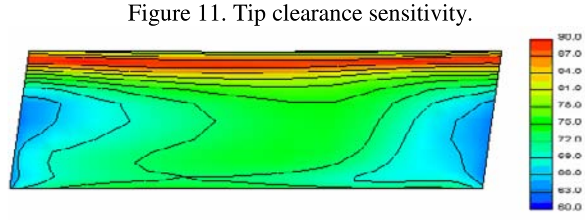

Figure 12. Absolute flow angle contour at rotor exit.

B. Diffuser Design

A vaned diffuser has become more popular because of its high efficiency feature compared with a vaneless diffuser. However, the problem with a conventional vaned diffuser design compressor lies in the fact that the operating range is often relatively small with a vaneless diffuser [2]. In order to overcome this problem, a low solidity vaned diffuser was proposed [2,15]. The low solidity diffuser research showed that a low solidity diffuser could provide not only a higher efficiency but also a reasonable operating flow range. As a remedy, different types of vane shape were tried for a low solidity diffuser. However most of the diffuser vane shapes were either derived from a NACA airfoil or just a flat plate [2, 15] and the applications of the low solidity vaned diffuser were limited in low pressure ratio machines. In this present study, in order to meet the higher efficiency and wide flow operating range requirements, a diffuser was designed to apply to this high-pressure ratio machine. The diffuser was generated by optimizing sections and stacking them up by using three-dimensional analyses [6,7].

In this design, the solidity of the diffuser is $\sigma = 0.7$. Given the solidity and inlet conditions, change of the vane number will cause to alter the length of the vane and the turning angle of the vane. The blade loading was thus changed. After the optimization study, the number of the diffuser vanes was set to nine, which gives a high efficiency and a better flow control.

In this study, three diffuser vane sections were designed and optimized for each section [7]. The diffuser vane airfoil sections were designed based on the inlet condition of impeller CFD analysis and the exit static pressure condition of the design requirements. After the design of each section, the diffuser blade was stacked-up based on three-dimensional analyses. The final diffuser was obtained after several optimization analyses. The typical mesh of the diffuser analysis at mid-span is shown in Fig. 13. The H-mesh was used and generated by employing different blocks. The design condition at mid-span pressure contour (Fig. 14) shows that there is a little incidence at the diffuser vane. This small incidence allows the compressor to have a wide operating range and have a relatively high efficiency at off-design conditions. The velocity vectors, Fig. 15, show that the flow field is well organized. There is no separation found in the design condition.

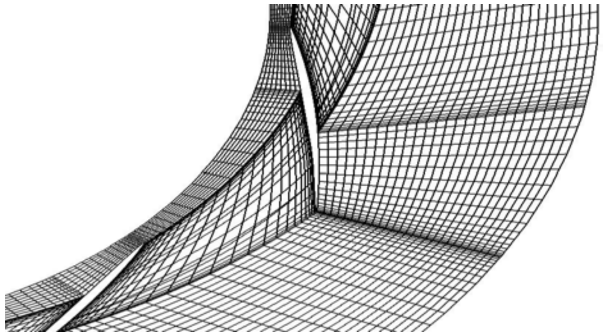

Figure 13. Mesh at the mid-span of the diffuser.

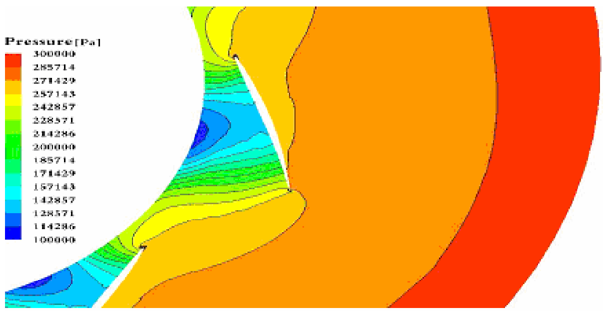

Figure 14. Static pressure contour at mid-span.

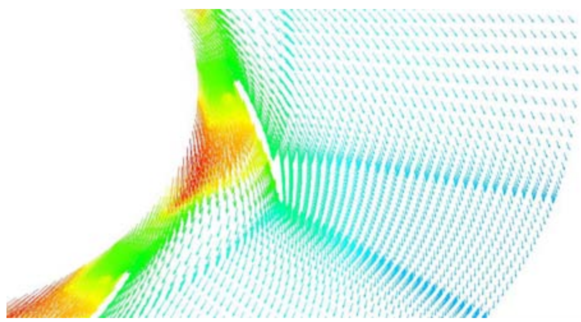

Figure 15. Velocity vector at mid-span.

C. Performance Prediction and Tests

The present compressor was designed by using a viscous design method by optimizing both efficiency and surge margin. In this design, the compressor performance was calculated by using the mean-line calculation and combination of the blockage and loss results from three-dimensional viscous flow analyses. The full machine CFD analysis only runs at three points, i.e. near surge design and near choke condition. The loss and blockage between three points were obtained using a linear relationship.

In CFD analysis, the structure hexahedral meshes are generated to define inlet pipe (541056 cells), impeller (541056 cells) and diffuser zones (541056 cells), while the unstructured tetrahedral cells are used to define the volute (470,614 cells) as shown in Fig. 16. The impeller stability operating range (SB) was defined from choke to a surge point. The choke point is simulated by reducing the backpressure with an increasing strength of the shock at either impeller inducer or diffuser vane throat. Stall is an unsteady phenomenon, which is impossible to simulate by using a steady flow analysis. However, the investigation of the stall inception by using the steady code can provide important information of the surge margin. In this analysis, the surge point is defined when the computation is not converged if the flow rate is reduced. The computational results are shown in Fig. 17 for the case of tip clearance of 2%.

The designed compressor stage was built and tested in an open loop test rig. Air was draw from ambient and discharge to ambient. The impeller was driven by an electric motor coupled with a gearbox. The test was performed at design impeller rotational speed and two different tip clearance settings were used, i.e. 2% and 5% of blade high. The mass flow rate of the compressor was measured at the discharge by a calibrated ASME nozzle [17]. The flow rate measurement uncertainty was within

2.0% and the speed was measured with a one pulse per revolution signal sensed by a magnetic probe, which looks to be a notch in the shaft. The measurement uncertainty of the speed was less than 0.01%, which has a very insignificant effect on the stage performance measurement. The temperatures were measured by using Type E half-shielded thermocouple. The uncertainty of the temperature measurement is about 0.25%. The measurement uncertainty for total pressure and static pressure are 0.25% and 0.15%, respectively. The inlet upstream and stage exit conditions were measured by employing five Kiel probes and five thermocouples at upstream of three time of impeller inlet pipe and discharge. Ten wall static pressure taps were used for the measurement of the inlet and discharge static pressure. The measurement results for the tip clearance effect are shown in Fig. 10. It is shown that variable tip clearance has a better effect on the rate of efficiency loss with increasing the tip clearance. The performance measurement is shown in Fig. 17. The experimental results show a good agreement with the calculations. Due to the stall phenomena during the test when the compressor is close to the stall, the vibration level increases. For the safety purpose of the bearing system, the test machine did not run to the machine surge. It was shown that except the flow close to choke range, the CFD provided a good estimate of the compressor performance. For the compressor flow close to chock, CFD provided more flow range than performance test. It is shown that the centrifugal compressor design procedure developed by this research provided a fairly successful design.

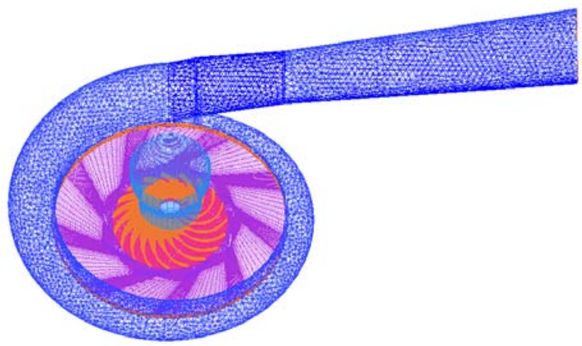

Figure 16. The computational mesh for compressor.

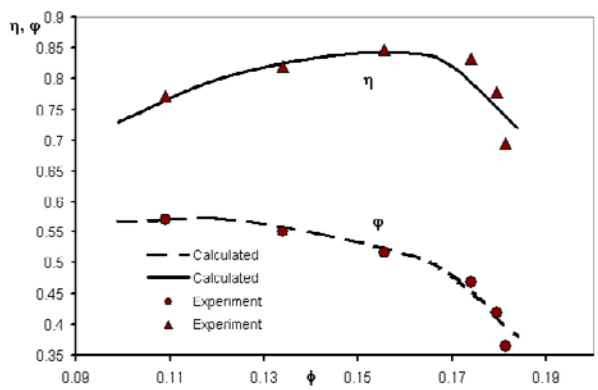

Figure 17. Compressor performance.

D. Volute

Figure 18 shows the static pressure distribution at mid span of the volute and diffuser. It can be seen that, for all the flow cases, the static pressure distributions near the vane diffuser inlet are symmetric and static pressures near volute inlet are distorted. The flow near choke presented the highest static pressure distortion at the inlet of the volute. The unsymmetrical pressure distributions inside the diffuser also cause the variations of the Mach number as shown in Fig. 19. The isentropic Mach number distributions show that, by increasing the compressor flow rate, the highest Mach number location moves downstream from vaneless diffuser to vaned diffusers. When the flow rate approaches closer to choke, the position of the highest Mach number moves toward the leading edge of the diffuser vanes. The diffuser vane inlet throat limited the maximum compressor flow, which causes a flow choke.

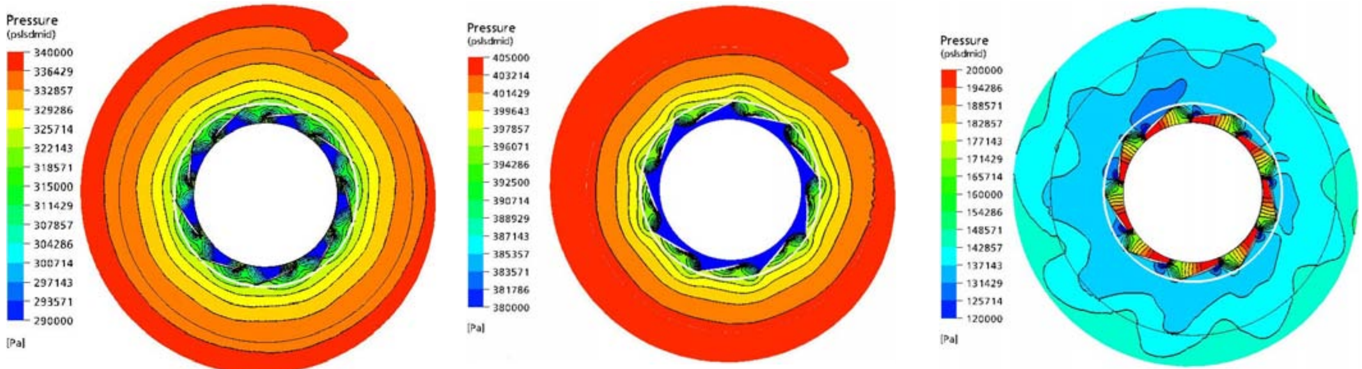

a. ϕ/ϕ_0 =1.08 b. ϕ/ϕ_0=0.7 c. ϕ/ϕ_0=1.25

Fig. 18 static pressure contours at mid-span.

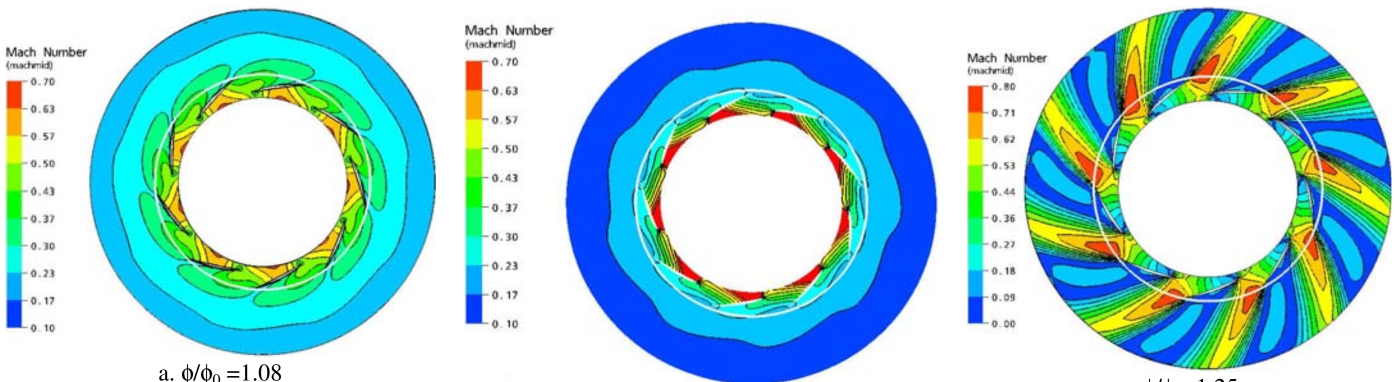

a. ϕ/ϕ_0 =1.08 b. ϕ/ϕ_0=0.7 c. ϕ/ϕ_0=1.25

Fig. 19 Mach number contours at mid-span.

III. Conclusions and Recommendations

A low flow coefficient high-pressure ratio single stage centrifugal compressor was designed by using a viscous optimization method. This compressor is capable of a high performance. A wide operating range was achieved without resorting to variable geometry and flow controls. The experimental results showed that the design is in good agreement with the test results. The applications of CFD provide the reliable design. It is proven that the design system developed in this study is feasible; the design thus provides a useful tool for a future centrifugal compressor development. The future development for this machine will be focused on the three-dimensional optimization of the impeller, and will introduce better material in order to build the impeller blades thinner and flow control investigation of impeller tip region.

Acknowledgments

The authors are thankful for NSF support on the numerical computation under CTS 020022N.

References

1. Japikse, D., 1996, “Centrifugal compressor design and performance”, Concepts ETI, VT, USA.
2. Amineni, N. K., and Engeda, A., 1997, “Pressure recovery in low solidity vaned diffusers for centrifugal compressors”, 97-GT-472.
3. Senoo, Y., Hayami, H. and Ueki, H., 1983, “Low solidity trandem cascade diffusers for wide flow range centrifugal blowers,” 83-GT-3.
4. Xu, C, Amano, R. S. and E. K. Lee, 2004, “ Investigation of an axial fan—Blade stress and vibration due to aerodynamic pressure field and centrifugal effects”, JSME International Journal, series b, vol. 47, No. 1, pp-75-90.
5. Kenny, D. P. 1984, “The history and future of the centrifugal compressor in aviation gas turbine”, 1st Cliff Garrett Turbomachinery Award Lecture, Society of Automotive Engineers, SAE/SP-804/602.
6. Xu, C. and Amano R.S., 2001, “On the Development of Turbine Blade Aerodynamic Design System,” ASME IGTI Turbo & Expo, 2001-GT-0443.

7. Xu, C and Amano, R. S., 2002, "Turbomachinery Blade Aerodynamic Design and Optimization," GT-2002-30541, 2002.
8. Weber C R, and Koronowski, M E, 1987, "Meanline performance prediction of volutes in Centrifugal compressors", ASME 31st Gas Turbine Conference and Exhibit, Dusseldorf, Germany, 86-GT-216.
9. Dong, R., Chu, S., and Katz, J., 1997, "Effect of Modification to Tongue and impeller Geometry on Unsteady Flow, Pressure Fluctuations and Noise in a Centrifugal Pump," ASME J. Turbomach., 119, PP. 506-515.
10. Arora, J.S., 1998, Introduction to Optimum Design, NY, MCGraw-Hill.
11. D. Bonaiuti, A. Arnone, M. Ermini, and L. Baldassarre, Analysis and Optimization of transonic centrifugal Compressor Impellers Using the Design of Experiments Technique, G T-2002-30619.
12. Xu, C. and Amano, R.S., "A Hybrid Numerical Procedure for Cascade Flow Analysis," *Numerical Heat Transfer*, Part B, 2000, Vol. 37, No. 2, pp. 141-164.
13. Xu, C. and Amano, R.S., "Computational Analysis Of Pitch-Width Effects On The Secondary Flows Of Turbine Blades," *Computational Mechanics*, Vol. 34, No. 2, 2004, pp. 111-120.
14. Harry, M. J., 1997, "The nature of Six Sigma quality,"
15. Senoo, Y., Hayami, H. and Ueki, H, 1983, "Low Solidity Tandem Cascade Diffusers for wide Flow Range Centrifugal Blowers," ASME paper, 83-GT-3.
16. CFX Ltd, 2003, "CFX5, version 5.6", UK
17. ASME, Performance Test Code on Compressors and Exhausters, PTC 10-97, 1997.